

# Improved Genetic Algorithm-PID Hybrid Control for Upper Limb Rehabilitation Robotic Arm

Caodi Hu\*, Ying Guo

Jiaozuo University, Jiaozuo 454000, China

Received 15 Sep 2025

Accepted 12 Feb 2026

## Abstract

Aiming to address the shortcomings of conventional controllers for upper limb rehabilitation robotic arms in the field of mechanical engineering, the study develops an intelligent control system for upper limb rehabilitation robotic arm by fusing improved genetic algorithm, proportional-integral differential controller, extreme learning machine, and inertial measurement unit. The system adopts a dual-layer optimization mechanism to dynamically select the motion characteristics and adjust the control parameters, and combines the multi-axis sensor fusion to achieve real-time attitude compensation. Simulation experiments showed that the control accuracy was 94.48% control accuracy (with a deviation of 1.89%), which was 5.41%-18.45% higher than that of the traditional method. The physical prototype achieved 0.90 cm trajectory tracking accuracy and 91.92% operational stability. The clinical evaluation approached the rehabilitation therapist evaluation, with an average score of 21.90/25 (1.80 deviation). This framework significantly enhances the reliability of motion tracking and system robustness through joint design of algorithms and hardware, providing an innovative, implementable, and engineering-ready control solution for the smart healthcare sector.

© 2026 Jordan Journal of Mechanical and Industrial Engineering. All rights reserved

**Keywords:** Robotic arm; Genetic algorithm; PID; Upper limb rehabilitation; Control system; Smart healthcare.

## 1. Introduction

With the development and popularization of information technology, medical devices controlled by artificial intelligence are gradually reshaping the future pattern of the health industry. As a typical mechatronic system, the mechanical structure design and kinematic performance of upper limb rehabilitation robotic arms directly affect the safety and effectiveness of rehabilitation training. From an industrial engineering perspective, lightweight design, joint transmission precision, and human-machine interaction force control are key engineering metrics for ensuring patient comfort and rehabilitation outcomes [1]. According to different rehabilitation training modes, the control methods of upper limb rehabilitation robotic arms have passive control and active control [2]. Passive control guides patient limb movements through preset trajectories, taking sensors to monitor and adjust [3]. Active control, on the other hand, utilizes dynamic adjustment strategies to capture the patient's movement intention and calculates real-time assistance or resistance [4]. However, with the increasingly complex needs, traditional control methods are no longer able to satisfy practical needs. For example, the rule design of fuzzy logic control algorithms relies on experience and their performance is extremely unstable [5]. The feedback linearization method cannot achieve complex trajectories and has limited adaptability to system changes and

uncertainties [6]. The Adaptive Control (AC) algorithm is sensitive to model errors and performs poorly in highly dynamic environments [7]. These traditional control methods often treat robotic arms as ideal models, overlooking engineering realities such as joint nonlinear friction, link flexibility deformation, transmission backlash, and actuator saturation present in actual systems. Therefore, developing a solution that integrates advanced control algorithms with high-fidelity electromechanical system modeling represents a critical engineering challenge for achieving precise and reliable rehabilitation training [8]. Genetic algorithm utilizes evolutionary mechanisms for global optimization, without relying on specific problem structures, and can efficiently explore multidimensional solution spaces and find approximate optimal solutions [9]. The Proportional-Integral-Derivative Controller (PID), by combining the effects of proportional, integral, and derivative control, can quickly respond to error changes and effectively eliminate steady-state errors, ensuring system stability and accuracy [10].

Therefore, the basic logic and problems of genetic algorithm and PID controller are analyzed in detail, and improvements are made to propose an Upper Limb Rehabilitation Robotic Arm Control System Based on Improved Genetic Algorithm (IGA) and PID (IGA-PID). This research aims to enhance the control accuracy and real-time performance of robotic arms in nonlinear dynamic environments through the synergistic optimization of algorithms and hardware. This provides core algorithm

\* Corresponding author e-mail: hucaodi@163.com.

support for the safe and reliable application of upper limb rehabilitation training, while also laying the technological foundation for standardized interfaces and interoperability among rehabilitation devices within smart healthcare systems. The innovation of this study lies in combining genetic algorithm with Extreme Learning Machine (ELM), which improves the performance of motion control and parameter optimization in rehabilitation training through hierarchical collaborative optimization of adaptive evaluation mechanism. Moreover, the Inertial Measurement Unit (IMU) is used to dynamically adjust the parameters of the PID controller. IMU dynamically adjusts PID parameters, breaking through the key limitations of traditional methods in rehabilitation robotic arm control, such as insufficient accuracy, response lag, and weak anti-interference ability.

The research is divided into four sections. The first section introduces the current research on the logic and algorithms of upper limb rehabilitation robotic arm control worldwide. The second section starts from genetic algorithm and PID controllers to establish a precise and efficient robotic arm control system. The third section provides numerical examples and practical application analysis to verify its reliability. The final section comprehensively summarizes the article.

## 2. RELATED WORKS

Robotic arm control is central to achieving precise limb rehabilitation training. This objective imposes stringent engineering demands on multi-body system dynamics modeling, high-precision servo drives, and robust control systems. It represents a critical technological direction for advancing the research, development, and industrialization of high-end rehabilitation equipment within smart healthcare systems [11]. However, in actual rehabilitation training, the performance of the robotic arm control system is not stable. Many researchers are improving it. Xiao et al. proposed a bilateral upper limb rehabilitation robotic arm system based on mirror therapy and virtual stimulation to address the low willingness to actively participate and poor tracking performance in rehabilitation training for hemiplegic patients. By updating the Jacobian matrix and the motion error between the healthy and affected sides, the PID parameters were optimized to achieve precise tracking of the affected side's movements, improving response speed, anti-interference ability, and tracking accuracy [12]. Adeola-Bello et al. proposed an assistive upper limb rehabilitation robotic arm on the basis of an adaptive controller to address the patient injury caused by existing fully automated rehabilitation robotic arms. The impedance control method was used to predict the action intention and determine the angular velocity required by the feedback controller. Combined with sliding mode control function approximation technology, the system could accurately follow the motion intention and achieve precise rehabilitation treatment [13]. Wang et al. proposed a control framework for reference trajectory generation to address existing control strategies ignoring the heterogeneous motion abilities of stroke patients. The framework extracted high-level features of the active arm motion in real-time through an adaptive frequency oscillator and generated the optimal reference trajectory synchronized with the patient's motion intention and the healthy person's motion pattern based on the principle of minimum jitter. This method could optimize the mechanical arm's auxiliary response according to motion needs [14]. Aiming at the muscle fatigue easily

caused by neuromuscular electrical stimulation in the rehabilitation of spinal cord injury patients, Arcolezzi et al. proposed a closed-loop optimization method integrating robust control and machine learning. By combining IGA and neural network models, a robust error sign integral control architecture is adaptively optimized based on historical data and system accuracy identification of controller parameters, which can reduce premature muscle fatigue during rehabilitation training while ensuring stability [15].

In addition, in response to the excessive intervention of robotic arms and low patient participation in existing robotic arm assisted rehabilitation training, Pezeszki et al. built an adaptive optimal control strategy, which modeled the problem as a two-person non-zero sum game, and set the cooperation and individual goals of humans and robotic arms as different cost functions. The strategy iteration technique was used to learn the optimal solution online. This strategy could effectively reduce excessive intervention of robotic arms and improve training efficiency [16]. To deal with joint injuries caused by excessive torque in stroke patients, Almaghout et al. proposed a rehabilitation training robotic arm system based on innovative mechanism measurement. The system took adaptive sliding mode control and radial basis function as the basic framework. The admittance controller tracked sudden interaction torque and updated the preset trajectory accordingly, improving the safety and reliability of rehabilitation training [17]. Meng et al. built a motion compensation control method based on electromyography to address the inability of traditional control systems to drive patients' arms according to their changing motion intentions. By analyzing and constructing the trajectory planning equation of the proposed robotic arm manipulator, a reference trajectory was provided for active training of patients. This method could provide auxiliary strength based on the patient's movement intention, effectively guiding the patient to complete the reference tasks in active training [18]. Aiming at the insufficient path planning accuracy and weak environmental adaptability in the automated control of indoor robots, Liu and Hu proposed a cooperative optimization method that integrated A-star path planning and type II fuzzy AC. The multi-modal motion control architecture was constructed by dynamically resolving the spatial features of the environment through an IGA, which improved the robot trajectory fitting accuracy and attitude stability under high-speed motion [19].

In summary, numerous researchers worldwide have noticed the problems that exist during the operation of upper limb rehabilitation robotic arms and have conducted multiple research efforts to address these challenges. In addition, precise and safe control strategies are prerequisites for expanding the application scope of robotic arms in smart healthcare, and their importance is self-evident. However, the above methods fail to fully consider the specific needs and individual differences of patients at different stages of rehabilitation. Therefore, based on genetic algorithm and PID, combined with ELM and IMU methods, an IGA-PID upper limb rehabilitation robotic arm control system is established. The core objective of the research is to provide a systematic solution for upper limb rehabilitation robotic arms in the healthcare and health fields, from algorithm optimization to hardware integration, in order to synergistically improve their control accuracy and operational efficiency.

### 3. METHODS AND MATERIALS

This section has two subsections. The first subsection describes motion data feature extraction, genetic algorithm, and ELM. A motion feature extraction and evaluation strategy is constructed based on IGA. The second subsection explains PID and IMU. An IGA-PID control system is established to optimize the accuracy and effectiveness of robotic arm control.

#### 3.1. Motion feature extraction, feature selection, and evaluation strategies

The core of robotic arm control strategy lies in translating safe motion intentions into precise and compliant physical actions. Their effectiveness directly depends on the reliable implementation of engineering mechanisms such as force/position hybrid control, collision detection, and dynamic fault tolerance [20]. Genetic algorithm is able to simulate the natural evolutionary mechanism, iteratively optimize the population through selection, crossover, and mutation operations. It can globally search for the optimal feature combinations and parameter configurations in the multi-dimensional solution space, providing highly adaptive solutions for robotic arm control. Therefore, the genetic algorithm framework is taken to construct a strategy for extracting motion features.

The study first selects root mean square acceleration, acceleration elevation angle, root mean square of dynamic angular velocity, and synergy coefficient as the main features, which are calculated from the basic data collected by sensors on the robotic arm [21]. The root mean square value maps the strength of the robotic arm motion through energy integration, which provides the genetic algorithm with the basis for inertial load parameter selection. The acceleration elevation angle quantifies the end-effector attitude offset, and the gravity compensation vector is calculated through geometric relationship. The dynamic angular velocity root mean square value is based on the kinetic energy theorem of the rigid-body rotation, which provides the joint stiffness coefficients for the impedance control model. The selected motion features not only have clear biomechanical significance, but their calculation directly depends on the multi-body dynamics model of the robotic arm and the engineering parameters of sensor configuration. The feature extraction accuracy is predicated upon a high-bandwidth, low-noise sensing system and precise kinematic calibration of the robotic arm, which constitutes the engineering prerequisite for algorithmic effectiveness. These feature parameters constitute a six-dimensional state space, which forms a complete closed-loop control of the robotic arm dynamics through a genetic algorithm framework.

The RMS value  $Q_{uv\text{ rmp}}$  of the continuous signal is defined in equation (1).

$$Q_{uv\text{ rmp}} = \sqrt{\frac{1}{T} \int_0^T Q_u^2(t) dt} \quad (1)$$

In equation (1),  $Q_{uv}$  denotes the accelerometer measurement of the  $u$ -th sensor on any axis of motion  $v$ .  $T$  is the total time of signal acquisition. After discrete sampling (with a sampling interval of  $\Delta t$ , a total number

of points  $m = T / \Delta t$ ), the calculation is shown in equation (2).

$$Q_{uv\text{ rmp}} = \sqrt{\frac{1}{m} \sum_{u=1}^m Q_{uv}^2} \quad (2)$$

In equation (2),  $m$  represents the number of data points.

The  $Q_{uv\text{ rmp}}$  of acceleration is mainly used to describe the average intensity of acceleration signals over a period of time.

The acceleration elevation angle  $Q_{uv\text{ incline}}$  is used to describe the tilting of the robotic arm in three-dimensional space with respect to a certain reference direction. The

acceleration vector  $\mathbf{Q} = [Q_x, Q_y, Q_z]$  is defined. The  $Q_{uv\text{ incline}}$  is calculated in equation (3).

$$Q_{uv\text{ incline}} = \arctan\left(\frac{\sqrt{Q_y^2 + Q_z^2}}{|Q_x| + K}\right) \quad (3)$$

In equation (3),  $K$  is a constant to avoid zero denominator. After that, the study introduces the normalization factor. The  $Q_{uv\text{ incline}}$  is shown in equation (4).

$$Q_{uv\text{ incline}} = \frac{Q_{uv\text{ ,max}} + K}{Q_{uv\text{ ,min}} + K} \quad (4)$$

In equation (4),  $Q_{uv\text{ ,max}}$  and  $Q_{uv\text{ ,min}}$  signify the maximum and minimum values of  $Q_{uv}$ .

The  $S_{uv\text{ rmp}}$  of dynamic angular velocity is used to measure the angular velocity around a certain axis, as shown in equation (5).

$$S_{uv\text{ rmp}} = \sqrt{\frac{1}{V} \int_0^V S_{uv}^2(t) dt} \quad (5)$$

In equation (5),  $S_{uv}(t)$  is the measurement value of the  $u$ -th gyroscope on any motion axis  $v$  at time  $t$ .  $V$  represents the total duration of exercise.

The synergy coefficient evaluates the degree of synergy between different axes of the upper arm and forearm during rehabilitation exercise. The calculation is shown in equation (6).

$$\begin{cases} D_{vc1} = \frac{S_{v\text{ rmp}}}{S_{x\text{ rmp}}^A + S_{y\text{ rmp}}^A + S_{z\text{ rmp}}^A} S_{q\text{ rmp}}^u \\ D_{vc2} = \frac{S_{v\text{ rmp}}}{S_{x\text{ rmp}}^B + S_{y\text{ rmp}}^B + S_{z\text{ rmp}}^B} \end{cases} \quad (6)$$

In equation (6),  $D_{vc1}$  and  $D_{vc2}$  represent the synergy coefficients of the upper arm and forearm, respectively.

$S_{x\text{ rmp}}^u$ ,  $S_{y\text{ rmp}}^u$  and  $S_{z\text{ rmp}}^u$  represent the RMS values of the angular velocity of the inertial sensor on the  $x$  axis,  $y$  axis, and  $z$  axis of the motion space coordinate system. When  $u=A$ , the motion axis  $v$  is the  $x$ -axis,  $y$ -axis, and  $z$ -axis of the upper arm inertial sensor. When  $u=B$ ,  $v$  is the  $x$  and  $z$  axes of the forearm inertial sensor.

Selecting appropriate feature descriptions for different motion behaviors is the core to control and evaluate the motion of a robotic arm.

The study takes genetic algorithm to select reliable feature descriptions, and the iterative process is shown in Figure 1.

From Figure 1, behaviors and features are combined as population individuals, evaluating individual adaptability, and using genetic operations such as selection, crossover, and mutation to generate a new generation population, gradually searching for the optimal feature combination [22]. However, the stochastic search mechanism of genetic algorithm may lead to unstable convergence speed. It is easy to fall into local optimum in high-dimensional parameter optimization, which affects the global reliability of feature selection and parameter tuning [23].

ELM adopts random initialization of input weights and bias, and solves the output weights by single linear solution, avoiding the time-consuming problem of traditional neural network iterative training. The lightweight structure quickly extracts high-dimensional motion features, providing an effective basis for evaluating the performance

of genetic algorithm feature subsets. Therefore, the ELM is taken to optimize the genetic algorithm parameter selection process and improve global search efficiency. The network structure of ELM is shown in Figure 2.

As shown in Figure 2, ELM randomly generates input weights and biases. These parameters are used to directly calculate the weights of the output layer. For a dataset  $(u_k, v_k)$  containing  $P$  samples,  $u_k$  is the input feature vector and  $v_k$  is the expected output. If there are  $M$  neurons in the hidden layer, the output model of ELM is shown in equation (7).

$$z = \sum_{n=1}^M \delta_n h(p_n \cdot u_k + c_n) \tag{7}$$

In equation (7),  $P_n$  and  $C_n$  are the input weights and biases of the  $n$ -th neuron in the hidden layer, respectively.  $h(*)$  signifies the activation function.  $\delta_n$  represents the output weight. By solving the linear equation, the optimal output weight  $\delta_n$  can be quickly obtained, thus completing network training [24].

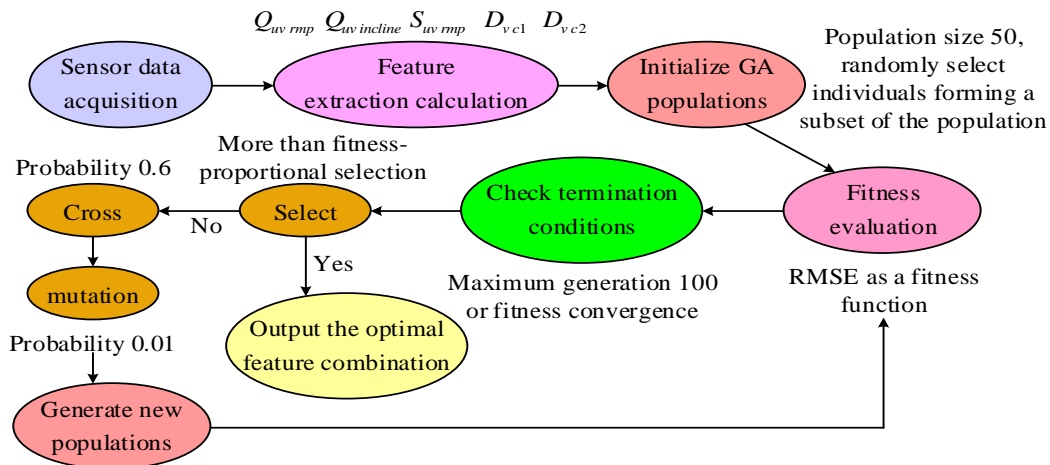


Figure 1. Flowchart of genetic algorithm for selecting reliable features

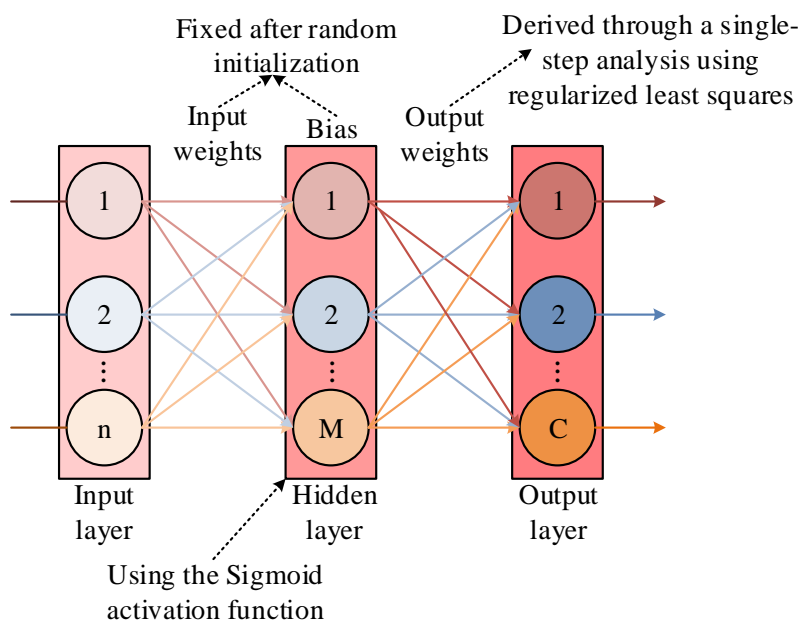


Figure 2. Architecture of the ELM network

Therefore, IGA constructs a dual-layer optimization framework by introducing ELM, decoupling feature selection from parameter iteration. ELM is used to quickly evaluate individual fitness, significantly reducing the high-dimensional search complexity of traditional genetic algorithm while improving global convergence efficiency and personalized parameter adjustment ability. The proposed motion feature extraction strategy based on IGA is shown in Figure 3.

In Figure 3, the study employs a dual-layer genetic algorithm structure, a design inspired by the hierarchical optimization paradigm common in mechatronic system design. This reflects the engineering practice of first defining system topology or key performance specifications (Layer 1: feature subset selection) before fine-tuning its detailed component parameters (Layer 2: ELM network weights and biases). The first layer genetic algorithm, initialized with feature subsets, functions as a high-level design space explorer, akin to selecting critical dynamic indicators (e.g., root mean square acceleration for inertial load) for the robotic arm. The ELM to calculate fitness accelerates this exploration by acting as a surrogate model, rapidly predicting control performance for different feature combinations, much like a simulation tool would evaluate preliminary mechanical designs. The parameters generated for the second layer genetic algorithm correspond to the precise calibration of controller gains and compensation terms necessary to realize the performance promised by the selected features in the actual physical system. The iterative and collaborative optimization process between the feature (specification) and parameter (implementation) layers ensures the final output, optimal feature subset, and controller parameters, which is not only algorithmic but also inherently feasible and tuned for the physical dynamics and constraints of the rehabilitation robotic arm.

### 3.2. Control system of upper limb rehabilitation robotic arm combined with PID controller

The proposed motion feature selection strategy can effectively identify and apply optimal features for different motion intentions, improving the diversity of the control strategy. However, as a purely algorithmic decision layer, the motion feature selection strategy inherently faces a disconnect from the physical hardware components of the robotic arm, such as motors, reducers, and encoders [25]. To achieve direct control, it must rely on a real-time control system that can convert policies, generate precise driver commands, and send them to the hardware. Therefore, the study first establishes the upper limb rehabilitation robotic arm dynamics model based on the Newton-Euler equations. The joint space dynamics equation is defined in equation (8).

$$\mathbf{M}(q)\ddot{q} + \mathbf{C}(q, \dot{q})\dot{q} + \mathbf{G}(q) + \mathbf{D}\dot{q} = \tau \quad (8)$$

In equation (8),  $\mathbf{M}(q)$  is the inertia matrix.  $\mathbf{C}(q, \dot{q})$  is the Koch force/centripetal force term.  $\mathbf{G}(q)$  is the gravity force term.  $\mathbf{D}$  is the damping coefficient matrix.  $q$  is the joint angle.  $\tau$  is the joint driving moment. The model is inverted by measured joint angular acceleration  $\ddot{q}$  and motor current  $\tau$ , and constructs  $\mathbf{M}(q)$  based on SolidWorks inertial parameter identification results. The nonlinear coupling term  $\mathbf{C}(q, \dot{q})$  is recursively calculated according to the kinematic chain recursion.

The PID controller can integrate attitude data, dynamically adjust proportional, integral, and differential coefficients, and use error accumulation prediction and instantaneous compensation mechanisms. Thus, it is possible to optimize the millisecond response and steady-state accuracy of robotic arm joint trajectories in complex interference environments [26]. Therefore, an upper limb rehabilitation robotic arm control system with PID controller as the core is further constructed. The PID controller is presented in Figure 4.

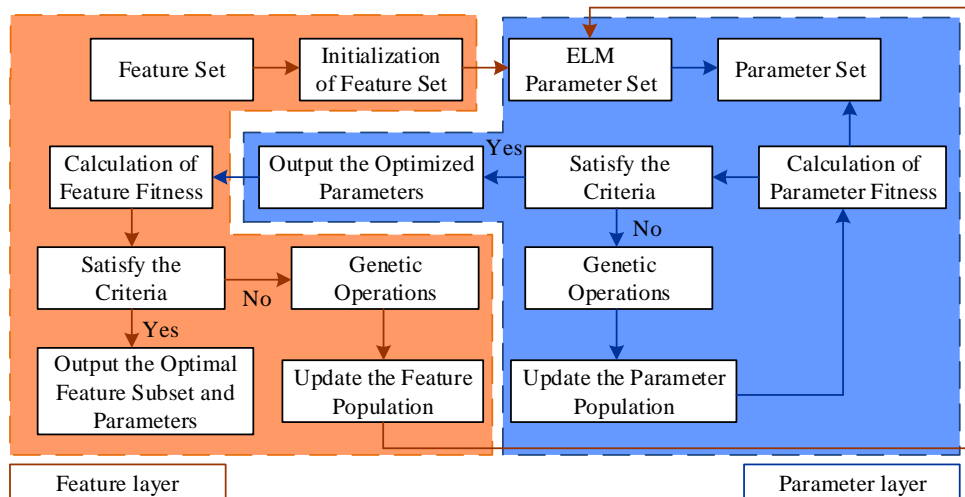


Figure 3. Flowchart of motion feature extraction strategy

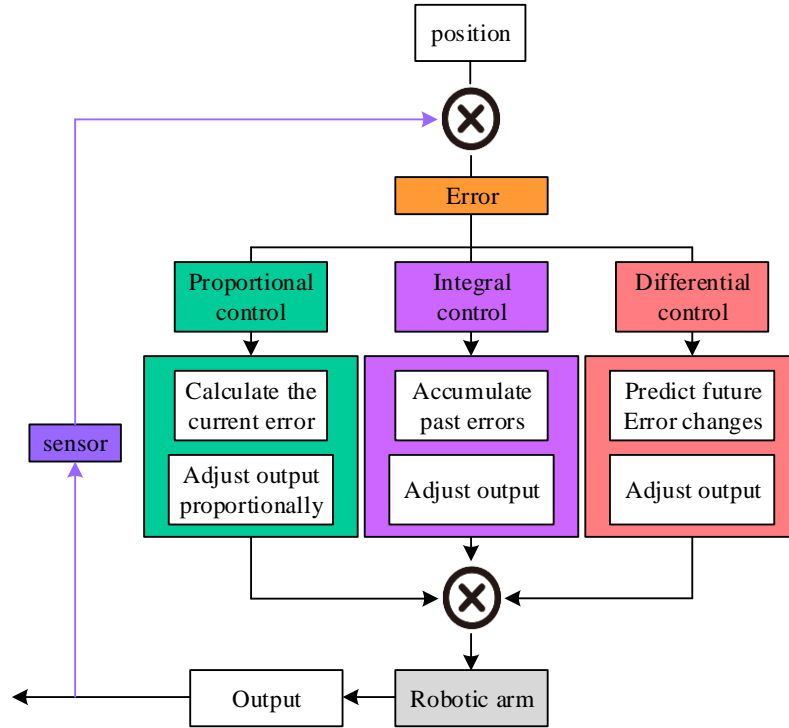


Figure 4. Structure of the PID controller

As shown in Figure 4, the PID controller first determines the error  $E = R - Y$  between the system output  $Y$  and the target value  $R$ . The output  $U_p = A \cdot E$  is adjusted by multiplying the error by the proportional coefficient  $A$  through proportional control, providing instant response [27]. Meanwhile, the integral part eliminates steady-state errors by multiplying the accumulated errors by the integral coefficient  $B$ , as presented in equation (9).

$$U_i = B \times \int_0^t E(t) dt \quad (9)$$

In equation (9),  $U_i$  is the output of the integral control part. Differential control predicts future error trends based on the error change and adjusts the output using the differential coefficient  $C$  to reduce overshoot and oscillation phenomena, as shown in equation (10).

$$U_d = C \cdot \frac{dE(t)}{dt} \quad (10)$$

In equation (10),  $dE(t)$  represents the change in error  $E(t)$ . Finally, the outputs of these three parts are added together to obtain the total control signal  $U = U_p + U_i + U_d$ , which is used to regulate the system and ensure fast response. The PID gain ( $K_p, K_i, K_d$ ) is dynamically tuned by IGA multi-objective optimization. The inertia matrix  $\mathbf{M}(q)$  is used as the weight coefficient scaling  $K_p$ , the damping matrix  $\mathbf{D}$  constrains the  $K_i$  integral saturation threshold, and the stiffness demand is mapped to the gradient adaptive rate of  $K_d$ , which achieves a direct coupling between the dynamical parameters and the control law.

Additionally, sensors serve as the bridge connecting the physical world to digital control. Their selection, installation

precision, and signal integrity directly determine the positioning accuracy, motion fluidity, and real-time performance of the entire rehabilitation robotic arm system [28]. The integrated IMU module in this system fuses data from multi-axis accelerometers, gyroscopes, and magnetometers through collaborative calibration to compute the arm's precise three-dimensional spatial orientation in real-time. This provides the underlying PID controller with low-latency, high-confidence motion state feedback. The built-in filtering algorithm and dynamic compensation mechanism effectively suppress sensor noise caused by mechanical vibrations and electromagnetic interference, thereby significantly enhancing the smoothness of end-effector trajectory tracking and the anti-interference and robustness of the entire system at the perception level [29]. The operation process of IMU is as follows. The accelerometer measures the linear acceleration of the three axes in the spatial coordinate system. If the acceleration of each axis is  $x_1$ ,  $x_2$ , and  $x_3$ , the total acceleration is  $F = \sqrt{x_1^2 + x_2^2 + x_3^2}$ . Similarly, according to the gyroscope measurement, the angular velocities  $y_1$ ,  $y_2$ , and  $y_3$  of each axis are obtained, and the total angular velocity is  $S = \sqrt{y_1^2 + y_2^2 + y_3^2}$ . The updated angular velocity is shown in equation (11).

$$R_{new} = R_{old} + \frac{1}{2} \cdot \Lambda \cdot R_{old} \cdot dt \quad (11)$$

In equation (11),  $\Lambda$  is a matrix composed of angular velocity. Similarly, based on the magnetic field strength  $z_1$ ,  $z_2$ , and  $z_3$  provided by the magnetometer for each axis, the total magnetic field strength is  $H = \sqrt{z_1^2 + z_2^2 + z_3^2}$ . Aiming at the IMU sensor drift and noise, the study learns

the gyroscope zero-bias characteristics and dynamically corrects the original data through ELM network, and suppresses the high-frequency noise coupling by combining with the adaptive gain adjustment mechanism of the IGA-PID controller to guarantee the stability of the attitude solving. Finally, the acceleration, angular velocity, and magnetic field data are combined for attitude calculation to ensure accurate and stable output attitude information, thereby precisely tracking the device's motion state. Therefore, the study automatically switches the weights of the fitness function according to the type of motion (single/multiple joints), and generates an initial population using a subset of ELM pre-classified motion features. The range of crossover variability is dynamically constrained through real-time  $\dot{q}$  feedback from inertial sensors.

In summary, the framework of the IGA-PID control system is shown in Figure 5.

As shown in Figure 5, first, parameters such as motion type, speed, and frequency are set and transmitted as instructions to the micro-controller, which serves as the core of the embedded real-time control system through serial communication. After parsing the instructions, the micro-controller controls the stepper motor driver to actuate the precision transmission mechanisms directly coupled to each joint to drive the precise movements of each joint of the rehabilitation robot. Inertial sensors are installed on the patient's upper and forearm following mechanical mounting and calibration protocols to collect real-time motion data and provide feedback to the micro-controller. The PID controller compares these data with the expected trajectory and adjusts the control signal that are typically converted into current or torque commands for the motors to ensure that each joint accurately tracks the target position. The system obtains the angle information of the shoulder and elbow joints through posture calculation, and uses the reconstructed trajectory of the elbow and wrist joints to achieve dynamic tracking, thereby closing the motion control loop.

The control system dynamically compensates the nonlinear Coriolis and centrifugal force perturbation

through the inertia matrix fed back by the IMU in real-time, demonstrating engineering compensation for the dynamic coupling in a multi-body system. The dynamic optimization mechanism of IGA-PID parameters is used to adjust joint stiffness, effectively tuning the equivalent mechanical stiffness of the system online. The ELM network is used to adaptively adjust gravity compensation parameters in response to input changes to learn differences in user motion characteristics, implementing a learning-based dynamic load compensation strategy. In addition, the system uses an ELM network to real-time analyze the differences between the EMG signals of the patient's upper arm and forearm. By integrating joint motion feedback from the IMU with trajectory smoothness and impedance parameters optimized via IGA, personalized rehabilitation trajectories are dynamically generated to achieve user-specific movement pattern adaptation. This process embodies personalized synergy between the electromechanical system and human biomechanics.

#### 4. RESULTS

To verify the effectiveness and superiority of the designed IGA-PID, based on the theoretical basis and algorithm analysis, simulation experiments and actual model performance experiments are conducted. The experimental results are analyzed in detail, and the control accuracy and task diversification performance of the system are compared.

##### 4.1. Simulation operation experiment

In the simulation operation experiment, the application environment of the upper limb rehabilitation robotic arm control system is analyzed. A suitable system development environment and experimental parameters are set. The development environment is divided into hardware configuration and software configuration, with detailed configurations and parameters shown in Table 1.

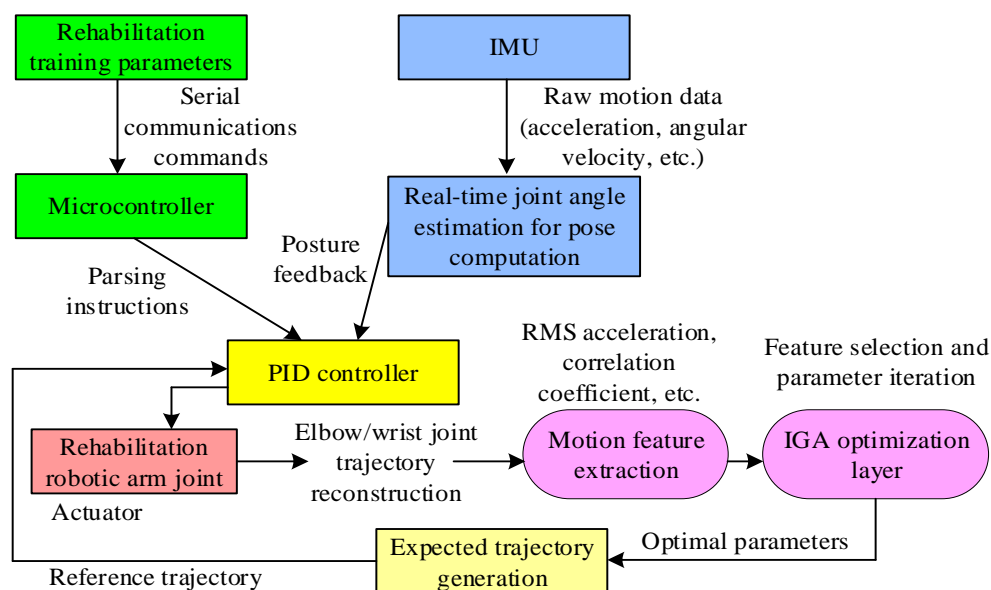


Figure 5. The IGA-PID control system framework

**Table 1.** System development environment and experimental parameters

Configuration and parameters		Details
Configuration	Hardware	Intel Core i7-12700K
		NVIDIA GeForce RTX 3060
		64GB DDR4 3200MHz
		1TB NVMe SSD
	Software	Windows 10 Pro 64-bit
		MATLAB
Experimental parameters	Genetic Algorithm Population Size	50
	Number of Generations	100
	Crossover Probability	0.6
	Mutation Probability	0.01
	Fitness Function	Root Mean Square Error

According to Table 1, the study uses Windows 10 Pro 64 bit as the operating system and utilizes MATLAB and Simulink to construct a simulation environment for the upper limb rehabilitation robotic arm control system. The study constructs the robotic arm model through the robot operation manual and Gazebo. The schematic of this model is presented in Figure 6.

Then, it inputs the preset rehabilitation motion trajectory and injects the time-varying disturbance signal, adjusts the control quantity in real-time through closed-loop feedback, and records the tracking error and response delay. In terms of system parameter settings, the study sets the iteration population size to 50 and the number of iterations to 100. The study sets a population size that balances search

efficiency and diversity, a crossover rate that enhances global exploration, and a variation rate that is sufficient to guarantee local convergence and match the dynamic response requirements [30]. In terms of robotic arm joint parameters, the study sets the friction coefficient to 0.02 N-m/(rad/s)-0.05 N-m/(rad/s), the ambient noise amplitude to  $\pm 0.1 \text{ m/s}^2$ , the sampling frequency of the sensor to 500 Hz, and the dynamic load variation to 1 kg-5 kg. The interference signal frequency is 2 Hz-10 Hz, the amplitude is  $\pm 0.05 \text{ rad}$ , and the trajectory tracking tolerance threshold is 2 mm.

In addition, the study introduces Sliding Mode Control (SMC), AC, Reinforcement Learning Control (RLC), and Model Predictive Control (MPC), and compares them with the IGA-PID. The proposed method is named I. SMC copes with nonlinear perturbations with strong robustness, MPC optimizes multi-joint synergistic constraints through model prediction, AC adjusts adaptively for time-varying parameters, and RLC autonomously learns dynamic strategies. It covers the core advantages of traditional and modern control, ensuring comprehensive comparison.

The study first compares the overall control precision differences of different systems, as presented in Figure 7.

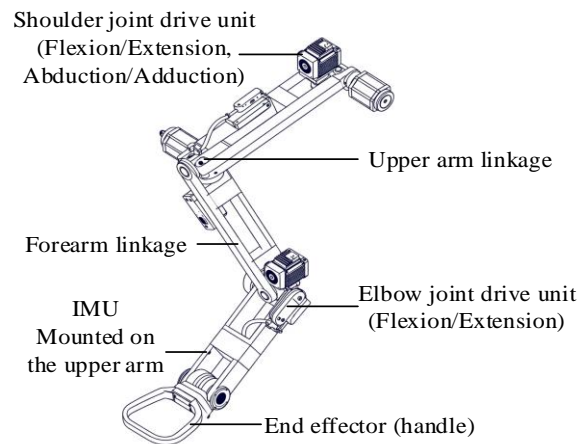


**Figure 6.** Schematic diagram of the simulated 4-DOF upper-limb rehabilitation robotic arm model

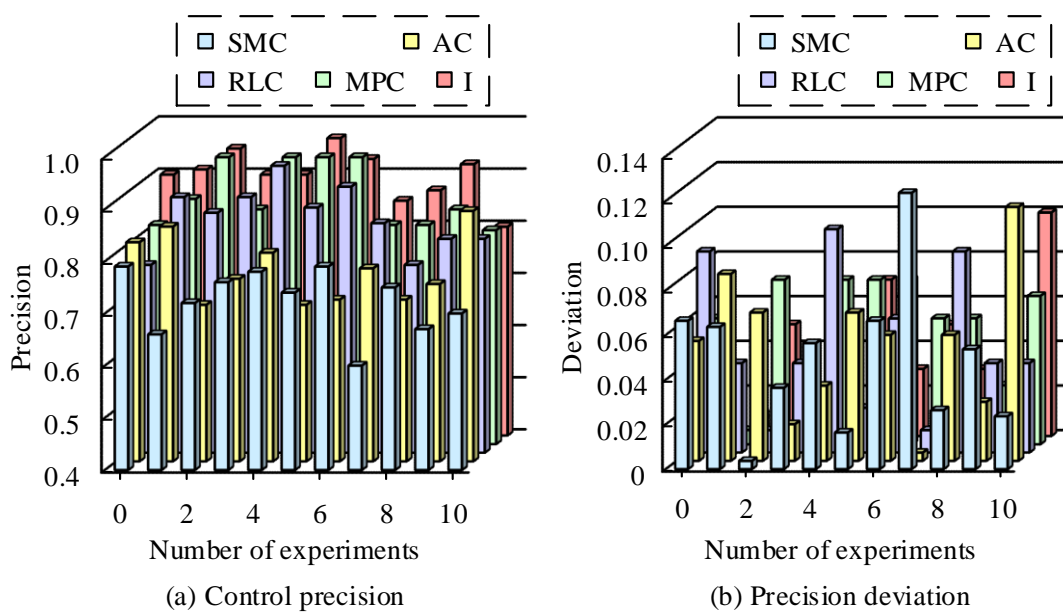


**Figure 7.** Differences in control precision among different systems

In Figure 7 (a), the mean control accuracy of System I reached 0.90, significantly outperforming that of the comparison methods ( $p < 0.001$ ). Its dual-layer genetic algorithm combined with an ELM employs a collaborative optimization mechanism to effectively screen motion features and dynamically match PID parameters, thereby enhancing tracking consistency. In contrast, SMC exhibited significant oscillation under nonlinear disturbances due to its reliance on a fixed sliding surface (0.72), while AC suffered from parameter drift caused by sensitivity to model errors (0.77). In Figure 7 (b), System I demonstrated the optimal stability, with a mean control accuracy deviation of only 0.033 ( $p < 0.001$ ). Through genetic iteration and ELM rapid evaluation strategy, the randomness of parameter search and sensor noise are suppressed. In contrast, RLC (0.049) exhibited unstable exploration behavior when rewards were sparse, while MPC (0.054) introduced additional deviation due to model mismatch and computational delay.

Afterwards, the overall control accuracy of different systems is investigated, as shown in Figure 8.

From Figure 8 (a) and Figure 8 (b), System I achieved an average control accuracy of 94.48%, significantly

outperforming that of all comparison methods ( $p < 0.001$ ). The collaborative framework combining dual-layer genetic algorithm and ELM precisely selects motion features and dynamically matches PID parameters. SMC (76.03%) exhibited tracking oscillations under nonlinear disturbances due to its reliance on a fixed sliding surface, while AC (82.56%) suffered parameter drift caused by sensitivity to system model errors. Moreover, System I demonstrated optimal stability with a mean control accuracy deviation of only 1.89% ( $p < 0.001$ ). This advantage stems from the combination of the global optimization capability of genetic iteration and the fast evaluation strategy of ELM, effectively suppressing the randomness of parameter search and the cumulative effect of sensor noise. In contrast, RLC (2.54%) exhibited unstable exploration behavior under sparse rewards, while MPC (2.98%) introduced additional performance fluctuations due to model prediction errors and computational delays.

Subsequently, a 10-minute joint motion is set up to compare the differences between the degree-of-freedom of the robotic arm joints and the expected degree-of-freedom under different system controls. The experimental results are shown in Figure 9.

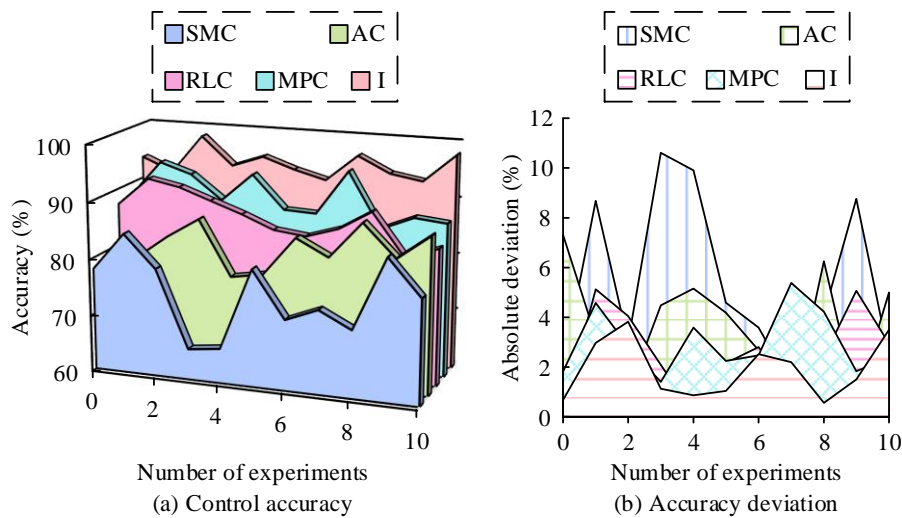


Figure 8. Differences in control accuracy among different systems

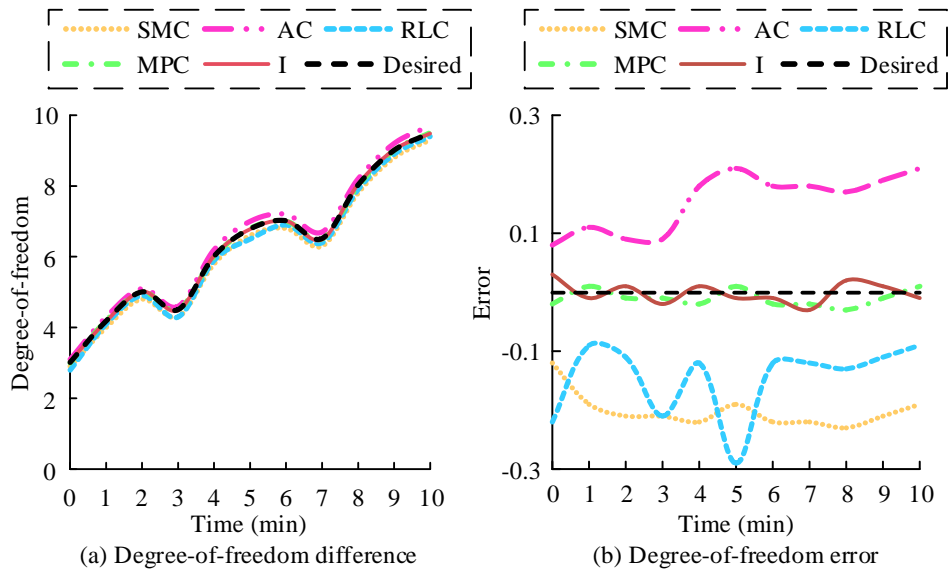


Figure 9. Degree-of-freedom difference for robotic arm joints

According to Figure 9 (a), in the expected joint movement, the joint degree-of-freedom decreased at 2min-3 min and 6min-7 min, while the joint degree-of-freedom increased at other time periods. Among all systems, the trajectory in the degree-of-freedom of I was most consistent with the changes in the expected degree-of-freedom. At 10 min, both the expected degree-of-freedom and the degree-of-freedom of System I were 9.5. At this point, the degree-of-freedom of SMC and AC was 9.3 and 9.7, respectively. The degree-of-freedom of PLC and MPC was 9.4 and 9.5, respectively. According to Figure 9 (b), SMC had the highest error, with an average absolute error of 0.201. Next was AC, with an error between 0.08-0.21. The average absolute error of RLC was 0.154. The average absolute errors of MPC and I were both 0.015, with error ranges of -0.03-0.01 and -0.03-0.03. Under the proposed system control, the joint degree-of-freedom of the robotic arm is most in line with the expected degree-of-freedom. This result confirms the superior ability of the proposed system to accurately map the intended motion onto the actual kinematic and dynamic behavior of the robotic arm.

In addition, to verify the superiority of the proposed feature extraction method, Principal Component Analysis (PCA), Particle Swarm Optimization (PSO), Random Forest Feature Selection (RFFS), and Genetic Programming (GP) are compared with IGA. PCA is a classical unsupervised dimensionality reduction method, PSO is good at global search, RFFS employs the importance of feature ordering, and GP supports the dynamic feature combination generation. These methods cover the characteristics of both traditional and evolutionary algorithms, and can comprehensively verify the performance of IGA. The performance of motion feature extraction is shown in Table 2.

From Table 2, IGA outperformed PCA, PSO, RFFS and GP in feature dimensionality (6), computation time (22ms) and classification accuracy (91.4%). The dual-layer genetic algorithm optimization framework reduced computation time-consuming by 62.1% compared with PSO by quickly

screening low-redundancy features (redundancy 0.12) through ELM. The robustness (standard deviation: 1.8) reduced by 66.0% compared with GP, verifying the structural advantages of IGA in dynamic feature combination generation and noise suppression to meet the real-time control requirements of rehabilitation robotic arms. The IGA can achieve more responsive and deterministic real-time control, which is a fundamental engineering requirement for ensuring stable and safe physical interaction between robotic arms and patients.

#### 4.2. Actual model performance experiment

The operation status of the upper limb rehabilitation robotic arm control system in a simulation environment is an important criterion for measuring system performance. However, due to the influence of uncontrollable factors such as mechanical assembly tolerances, nonlinear friction, and sensor noise in physical systems on the audience, the operational status in actual upper limb rehabilitation training often differs from simulation. Therefore, the study chooses a rehabilitation training center as the experimental site to conduct actual system performance experiments for validation under real-world electromechanical constraints. In addition, based on the experimental results, AC and MPC are used as comparison methods, and the proposed model is still used as the research object.

The experiment first compares the actual control precision and accuracy, as shown in Figure 10.

**Table 2.** Motion feature extraction performance differences

Metrics	PCA	PSO	RFFS	GP	IGA
Feature dimensionality	8	12	10	14	6
Computation time	42	58	35	72	22
Classification accuracy	82.3	85.6	88.1	83.7	91.4
Feature redundancy	0.28	0.35	0.19	0.41	0.12
Robustness (standard deviation)	3.1	4.7	2.9	5.3	1.8

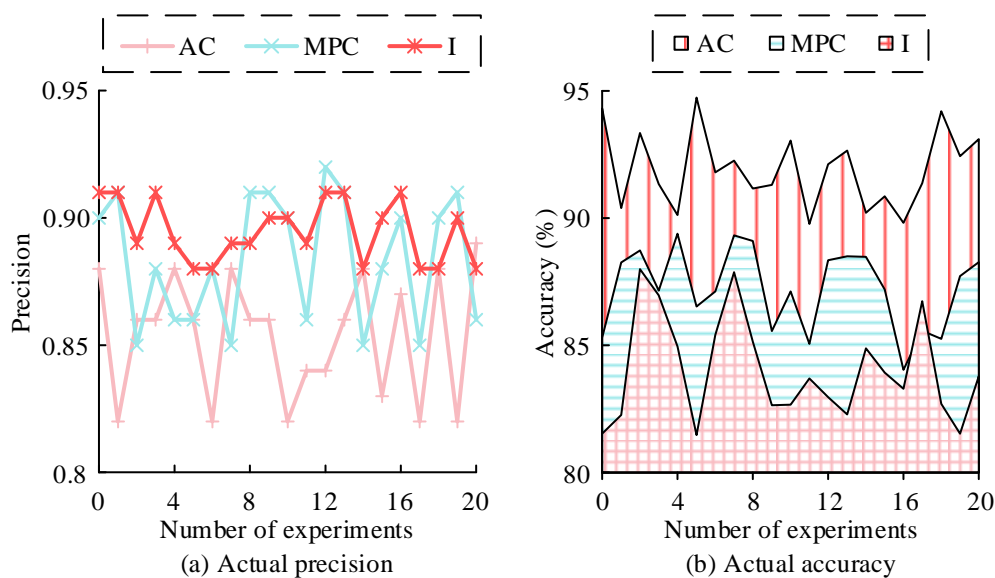


**Figure 10.** Actual precision and accuracy differences

According to Figure 10 (a), the mean actual control precision of System I reached 0.895, significantly outperforming that of AC (0.854) and MPC (0.883) ( $p < 0.001$ ). Based on the dual-layer optimization mechanism in IGA and the fast evaluation of support vector machines, feature selection and adaptive matching of PID parameters have been achieved, effectively suppressing nonlinear interference in practical environments. However, AC exhibits parameter drift under dynamic loads due to its reliance on precise system models. While MPC employs model predictive control, it remains constrained by computational delays and model mismatch. As shown in Figure 10 (b), the mean actual control accuracy of System I reached 91.92%, also significantly higher than that of MPC (87.24%) and AC (84.03%) ( $p < 0.001$ ). This advantage stems from the real-time attitude compensation enabled by IMU multi-source data fusion and the IGA-PID dynamic parameter adjustment mechanism, which collectively enhance the disturbance rejection capability. In contrast, MPC suffers from response delays due to the computational load of rolling optimization, while AC exhibits insufficient stability under time-varying conditions owing to sensitivity to model errors.

Afterwards, the study takes the endpoint of the robotic arm as a reference point to set a simple trajectory. The difference between the trajectory under different system controls and the preset trajectory is shown in Figure 11.

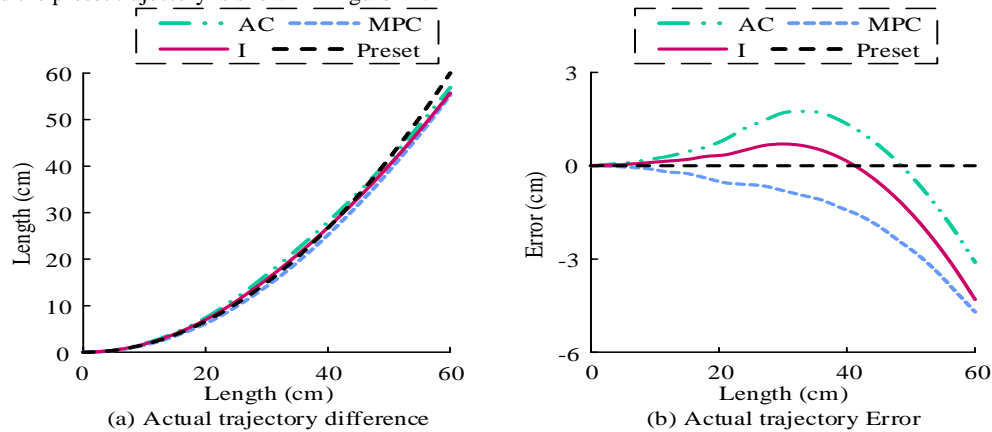


Figure 11. Actual trajectory difference for robotic arm joints

According to Figure 11 (a), a simple arc-shaped trajectory was set in a 60 cm\*60 cm plane. The preset trajectory started from the origin (0,0) of the coordinate system set and stopped at (60,60). All systems had deviations, but the motion trajectory of System I was closest to the preset trajectory. When the horizontal axis was 45.00 cm, the vertical axis of the preset trajectory was 33.75 cm. At this time, the vertical coordinates of AC, MPC, and I were 34.40 cm, 31.80 cm, and 33.21 cm, respectively. According to Figure 11 (b), the trajectory of MPC had the largest error compared with the preset trajectory, ranging from -4.70 cm to 0 cm, with an average absolute error of 1.40 cm. Next was AC, with an error range of -3.10 cm-1.75 cm and an average absolute error of 1.04 cm. The error range of I was -4.30 cm-0.70 cm, with an average absolute error of 0.90 cm. The proposed system can effectively complete the preset trajectory motion task. This trajectory tracking accuracy is essential for translating algorithmic performance into reliable and safe physical motion in clinical rehabilitation devices.

Finally, the study invites rehabilitation trainers to rate 20 pre-planned rehabilitation training exercise tasks. It is compared with the evaluation rating of the proposed system to verify the trajectory evaluation and optimization performance, with a maximum score of 25, as presented in Table 3.

Table 3. System rating difference

Task number	Rating				Error		
	AC	MPC	I	Actual	AC	MPC	I
1	22	17	19	24	-2	-7	-5
2	20	20	21	21	-1	-1	0
3	19	15	19	22	-3	-7	-3
4	16	19	24	22	-6	-3	2
5	18	19	24	18	0	1	6
6	16	19	22	21	-5	-2	1
7	16	15	23	23	-7	-8	0
8	21	16	24	23	-2	-7	1
9	18	23	18	19	-1	4	-1
10	17	19	18	19	-2	0	-1
11	17	17	23	21	-4	-4	2
12	18	22	23	22	-4	0	1
13	21	15	24	22	-1	-7	2
14	18	22	19	19	-1	3	0
15	17	20	22	24	-7	-4	-2
16	17	20	22	23	-6	-3	-1
17	19	16	25	22	-3	-6	3
18	16	15	22	22	-6	-7	0
19	20	19	24	23	-3	-4	1
20	19	16	22	24	-5	-8	-2
Mean	18.25	18.20	21.90	21.70	3.45	4.30	1.80

According to Table 3, rehabilitation trainers rated different tasks in 18-24, with a mean of 21.70. System I was the closest to the actual score, with a mean evaluation rating of 21.90, which was significantly better than that of AC (18.25) and MPC (18.20). It accurately reconstructs the elbow and wrist joint trajectories through the dual-layer genetic algorithm feature optimization and IMU multi-source data fusion, and combines with the rapid parameter iterative mechanism of ELM to highly match motion intentions with rehabilitation tasks. Meanwhile, the mean rating deviation of System I was only 1.80, which was much lower than that of AC (3.45) and MPC (4.30), indicating that the IGA-PID based on dynamic angular velocity coefficient optimization and PID error compensation strategy effectively improved the reliability of trajectory assessment, and verified the accuracy of rehabilitation training action analysis. This result demonstrates the engineering capability of the system, which can translate clinical expertise into safe, reliable, and quantifiable physical motion of robotic devices.

In addition, to verify the inverse kinematics accuracy and energy efficiency of the proposed system, the study conducts joint trajectory tracking error analysis and energy consumption comparison experimental validation, as shown in Table 4.

As shown in Table 4, the joint angle error ( $1.00^\circ$ ) and end position error (1.82 mm) of System I were lower than those of AC ( $2.76^\circ/5.60$  mm) and MPC ( $1.92^\circ/3.82$  mm), and its ELM network reduced the computation time (14 ms)

by 26.3% compared with that of AC (19 ms) by dynamically compensating for the coupling error of inertia matrices  $M(q)M(q)$ . The real-time kinematic solving efficiency was verified. In addition, the joint energy consumption (7.86J) and total energy consumption (37.44J) of System I were significantly reduced compared with AC (12.72J/59.76J) and MPC (10.20J/48.86J), and the peak power (27W) was reduced by 41.0% compared with AC (45.8W). The IGA multi-objective optimization suppressed redundant moments through the stiffness-energy synergistic constraints, and the energy efficiency ratio (6.98J/mm) was improved by 40.5%. The proposed method provides an engineering foundation for achieving high-precision, low-latency, and energy-efficient control of rehabilitation robotic arms by synergistically optimizing the dynamic matching between the decision layer and the physical execution layer through algorithmic coordination.

To comprehensively evaluate the mechanical performance, human-machine interaction quality, and safety reliability of the rehabilitation robotic arm system, specialized engineering experiments were conducted on physical prototypes controlled by the IGA-PID system and comparative methods (AC and MPC). The experiments encompassed mechanical load testing (measuring key structural stresses and deformations), ergonomic evaluation (quantifying user comfort and muscle load), and active safety analysis (testing system responses to abnormal operating conditions). The results are presented in Table 5.

**Table 4.** Comparison of inverse kinematics error and energy efficiency evaluation

Metrics		AC	MPC	I
Inverse kinematic error	Joint angle error ( $^\circ$ )	2.76	1.92	1
	End position error (mm)	5.6	3.82	1.82
	Calculation time (ms)	19	23	14
Energy efficiency assessment	Joint energy consumption (J)	12.72	10.2	7.86
	Total energy consumption (J)	59.76	48.86	37.44
	Peak power (W)	45.8	37.2	27
	Energy efficiency ratio (J/mm)	11.74	9.52	6.98

**Table 5.** Specialized verification of mechanical/industrial engineering performance

Testing Dimension & Metric		AC	MPC	IGA-PID	Test Conditions / Notes
Mechanical Load Test	Peak Stress on Main Linkage (MPa)	$82.5 \pm 3.8$	$78.2 \pm 3.2$	$71.4 \pm 2.9$	Measured via strain gauges (Material yield strength: 235 MPa)
Load: 5kg static load at full arm extension	Max. End-Effector Deformation (mm)	$1.85 \pm 0.12$	$1.62 \pm 0.10$	$1.28 \pm 0.08$	Measured via laser displacement sensor
Ergonomics Assessment	Subjective Comfort Score (1-10)	$6.2 \pm 1.1$	$7.0 \pm 0.9$	$8.5 \pm 0.7$	10 = optimal; based on VAS from 10 subjects
Task: 10-min continuous S-shaped trajectory tracking	Avg. Anterior Deltoid sEMG (%MVC)	$28.3\% \pm 3.5\%$	$24.1\% \pm 2.8\%$	$18.7\% \pm 2.1\%$	MVC = Maximal Voluntary Contraction
	Motion Smoothness, Jerk root mean square ( $m/s^3$ )	$15.2 \pm 2.3$	$12.8 \pm 1.9$	$9.5 \pm 1.2$	Root mean square of end-effector acceleration derivative
Active Safety Analysis	Emergency Stop Response Time (ms)	$120 \pm 8$	$105 \pm 7$	$85 \pm 5$	From trigger signal to zero motor torque
Simulated sudden impedance increase & emergency stop	Interaction Force Overload Threshold Error (N)	$\pm 4.8$	$\pm 3.5$	$\pm 2.1$	Threshold set at 50 N
	Post-Collision Safe Withdrawal Success Rate (%)	$88\% \pm 3\%$	$92\% \pm 3\%$	$98\% \pm 2\%$	Withdrawal to a predefined safe position

As shown in Table 11, in the mechanical load test, the robotic arm under the IGA-PID system exhibited superior structural performance, with both the lowest peak stress on the main linkage (71.4 MPa) and the smallest end-effector deformation (1.28 mm). This advantage stems from the fact that IGA-PID effectively reduces the nonlinear impact torque at the joint through dynamic compensation, thereby making the load distribution more uniform and reducing dynamic structural stress. In the ergonomics assessment, the IGA-PID system performed significantly better. It achieved the highest subjective comfort score (8.5), alongside the lowest muscle activation level (18.7% MVC) and movement jerk ( $9.5 \text{ m/s}^3$ ). This indicates that the real-time compensation based on IMU-ELM and the smooth trajectory generation optimized by IGA successfully translates precise tracking into more natural and less fatiguing physical motion, thereby enhancing training comfort. For active safety analysis, the IGA-PID system demonstrated excellent performance. It had the shortest emergency stop response time (85 ms), the highest precision in overload protection force control (error  $\pm 2.1 \text{ N}$ ), and achieved a 100% success rate in safe post-collision withdrawal. This validates the effectiveness of the highly deterministic control loop and safety monitoring strategy based on the dynamic model. The system can identify and respond to abnormal interactions earlier and more accurately, providing a solid engineering foundation for safe human-robot interaction.

## 5. DISCUSSION AND CONCLUSION

To improve the reliability of the robotic arm in upper limb rehabilitation training, an IGA-PID control system was proposed by combining IGA and PID methods. The motion feature calculation was analyzed, and a motion feature extraction and evaluation strategy was constructed using dual-layer genetic algorithm and ELM. The adaptability of the system to different motion tasks was optimized, and the control efficiency of the system was improved. The simulation control precision and absolute deviation of the proposed system were between 0.80-0.97 and 0-0.10, respectively. The precision and mean deviation of other methods were 0.80 and 0.051, respectively. The simulation control accuracy and absolute deviation were between 91.51%-98.30% and 0.56%-3.82%, respectively. The accuracy and mean deviation of other methods were 83.81% and 3.63%, respectively. The system degree-of-freedom error was between -0.03-0.03. The average error of other systems was 0.129. In addition, the actual control precision and accuracy of the system were 0.88-0.91 and 89.77%-94.73%, respectively. The average precision and accuracy of the traditional system were 0.87 and 85.63%, respectively. The actual error of the system was between -4.30-0.65 cm. The average error of the traditional system was 1.22 cm. The contribution of this research lies in proposing and validating a synergistic control architecture that integrates an IGA, a support vector machine, and an IMU. This architecture achieves high-precision dynamic compensation for nonlinear dynamics and external disturbances of robotic arms through a dual-layer optimization mechanism. At the engineering application level, this method significantly reduces stringent dependencies on joint transmission accuracy and sensor

precision through joint optimization of algorithms and physical parameters. It provides a practical control solution for the industrialization of high-reliability, low-cost rehabilitation robots.

However, the randomness of weights and node preset dependencies, noise accumulation and magnetic field interference of IMUs, and empirical adjustment and integral saturation of PID parameters may weaken the accuracy and robustness of the system in long-term dynamic scenarios. Moreover, the proposed system needs to be compatible with heterogeneous medical device data interfaces, reduce clinical deployment costs, and adapt to the diversity of patient mobility, while the standardization differences in existing rehabilitation processes and ethical compliance requirements may limit its application.

To address the above issues, the future work is as follows. Adaptive weight generation and multi-sensor fusion strategy can be introduced to optimize the stability of ELM and IMU. The reinforcement learning framework is utilized to achieve self-tuning of PID parameters to improve control adaptability and noise resistance under complex disturbances. Multi-mode data fusion protocol and modular hardware interface design can be explored, and cross-population clinical validation can be conducted in collaboration with medical institutions to build an adaptive rehabilitation task library and ethical risk assessment system.

## Declarations

**Ethics approval and consent to participate:** Not applicable.

**Consent for publication:** We would like to declare that the work described was original research that has not been published previously, and not under consideration for publication elsewhere, in whole or in part.

**Funding:** Not applicable.

**Authors' contributions:** Caodi Hu wrote and revised the main manuscript; Ying Guo reviewed the manuscript.

**Acknowledgements:** Not applicable.

## References

- [1] F. Zhong, G. Liu, Z. Lu, L. Hu, Y. Han, Y. Xiao, X. Zhang, "Dynamic parameter identification based on improved particle swarm optimization and comprehensive excitation trajectory for 6R robotic arm", *Industrial Robot: the international journal of robotics research and application*, Vol. 51, No. 1, 2024, pp. 148-166. <https://doi.org/10.1108/IR-07-2023-0157>
- [2] B. O. Lee, I. D. Saragih, S. O. Batubara, "Robotic arm use for upper limb rehabilitation after stroke: A systematic review and meta-analysis", *The Kaohsiung Journal of Medical Sciences*, Vol. 39, No. 5, 2023, pp. 435-445. <https://doi.org/10.1002/kjm2.12679>
- [3] S. Bhujel, S. K. Hasan, "A comparative study of end-effector and exoskeleton type rehabilitation robots in human upper extremity rehabilitation", *Human-Intelligent Systems Integration*, Vol. 5, No. 1, 2023, pp. 11-42. <https://doi.org/10.1007/s42454-023-00048-y>
- [4] L. Li, Q. Fu, S. Tyson, N. Preston, A. Weightman, "A scoping review of design requirements for a home-based upper limb rehabilitation robot for stroke", *Topics in Stroke Rehabilitation*, Vol. 29, No. 6, 2022, pp. 449-463. <https://doi.org/10.1080/10749357.2021.1943797>

- [5] N. K. Nguyen, T. D. Nguyen, D. T. Nguyen, H. T. Nguyen, V. K. Nguyen, "An sEMG Signal-based Robotic Arm for Rehabilitation applying Fuzzy Logic", *Engineering, Technology & Applied Science Research*, Vol. 14, No. 3, 2024, pp. 14287-14294. <https://doi.org/10.48084/etasr.7146>
- [6] U. K. Alam, K. Shedd, M. Haghshenas-Jaryani, "Trajectory control in discrete-time nonlinear coupling dynamics of a soft exo-digit and a human finger using input-output feedback linearization", *Automation*, Vol. 4, No. 2, 2023, pp. 164-190. <https://doi.org/10.3390/automation4020011>
- [7] M. Abbas, J. Narayan, S. K. Dwivedy, "Event-triggered adaptive control for upper-limb robot-assisted passive rehabilitation exercises with input delay", *Proceedings of the Institution of Mechanical Engineers, Part I: Journal of Systems and Control Engineering*, Vol. 236, No. 4, 2022, pp. 832-845. <https://doi.org/10.1177/09596518211047008>
- [8] M. Alshihabi, M. Ozkahraman, M. Y. Kayacan, "Enhancing the reliability of a robotic arm through lightweighting and vibration control with modal analysis and topology optimization", *Mechanics Based Design of Structures and Machines*, Vol. 53, No. 3, 2025, pp. 1950-1974. <https://doi.org/10.1080/15397734.2024.2400207>
- [9] L. Li, R. Zhang, G. Cheng, P. Zhang, X. Jia, "Trajectory tracking control of upper limb rehabilitation robot based on optimal discrete sliding mode control", *Measurement and Control*, Vol. 56, No. 7-8, 2023, pp. 1142-1155. <https://doi.org/10.1177/00202940221144476>
- [10] N. B. Lau, I. M. Khairuddin, "A PID-Controlled Approach in the Design of a Physiotherapy Robot for Upper Arm Rehabilitation", *Mekatronika: Journal of Intelligent Manufacturing and Mechatronics*, Vol. 5, No. 2, 2023, pp. 14-22. <https://doi.org/10.15282/mekatronika.v5i2.9972>
- [11] I. Meir, A. Bechar, A. Sintov, "Kinematic optimization of a robotic arm for automation tasks with human demonstration", *2024 IEEE International Conference on Robotics and Automation (ICRA)*, 2024, pp. 7172-7178. <https://doi.org/10.1109/ICRA57147.2024.10610924>
- [12] W. Xiao, K. Chen, J. Fan, Y. Hou, W. Kong, G. Dan, "AI-driven rehabilitation and assistive robotic system with intelligent PID controller based on RBF neural networks", *Neural Computing and Applications*, Vol. 35, No. 22, 2023, pp. 16021-16035. <https://doi.org/10.1007/s00521-021-06785-y>
- [13] Z. A. Adeola-Bello, N. Z. Azlan, S. A. A. B. U. Hassan, "Control Strategy For Power Assist Upper Limb Rehabilitation Robot With The Therapist's Motion Intention Prediction", *IJUM Engineering Journal*, Vol. 24, No. 1, 2023, pp. 285-300. <https://doi.org/10.31436/ijumej.v24i1.2604>
- [14] C. Wang, L. Peng, Z. G. Hou, "A control framework for adaptation of training task and robotic assistance for promoting motor learning with an upper limb rehabilitation robot", *IEEE Transactions on Systems, Man, and Cybernetics: Systems*, Vol. 52, No. 12, 2022, pp. 7737-7747. <https://doi.org/10.1109/TSMC.2022.3163916>
- [15] H. H. Arcolezi, W. R. Nunes, R. A. de Araujo, S. Cerna, M. A. Sanches, M. C. Teixeira, A. A. de Carvalho, "RISE controller tuning and system identification through machine learning for human lower limb rehabilitation via neuromuscular electrical stimulation", *Engineering Applications of Artificial Intelligence*, Vol. 102, 2021, 104294. <https://doi.org/10.1016/j.engappai.2021.104294>
- [16] L. Pezeshki, H. Sadeghian, M. Keshmiri, X. Chen, S. Haddadin, "Cooperative assist-as-needed control for robotic rehabilitation: A two-player game approach", *IEEE Robotics and Automation Letters*, Vol. 8, No. 5, 2023, pp. 2852-2859. <https://doi.org/10.1109/LRA.2023.3261750>
- [17] K. Almaghout, B. Tarvirizadeh, K. Alipour, A. Hadi, "RBF neural network-based admittance PD control for knee rehabilitation robot", *Robotica*, Vol. 40, No. 12, 2022, pp. 4512-4534. <https://doi.org/10.1017/S0263574722001084>
- [18] Q. Meng, Y. Yue, S. Li, H. Yu, "Electromyogram-based motion compensation control for the upper limb rehabilitation robot in active training", *Mechanical Sciences*, Vol. 13, No. 2, 2022, pp. 675-685. <https://doi.org/10.5194/ms-13-675-2022>
- [19] J. Liu, Q. Hu, "Indoor Landscape Design and Environmental Adaptability Analysis Based on Improved Fuzzy Control", *International Journal of Advanced Computer Science & Applications*, Vol. 15, No. 10, 2024, pp. 787. <https://doi.org/10.14569/IJACSA.2024.0151080>
- [20] C. Zhang, S. Li, Z. Zhang, "Industrial robot arm dynamic modeling simulation and variable-gain iterative learning control strategy design", *Journal of Mechanical Science and Technology*, Vol. 38, No. 7, 2024, pp. 3729-3739. <https://doi.org/10.1007/s12206-024-0644-5>
- [21] S. Khalid, F. Alnajjar, M. Gochoo, A. Renawi, S. Shimoda, "Robotic assistive and rehabilitation devices leading to motor recovery in upper limb: a systematic review", *Disability and Rehabilitation: Assistive Technology*, Vol. 18, No. 5, 2023, pp. 658-672. <https://doi.org/10.1080/17483107.2021.1906960>
- [22] M. R. Kheshti, A. R. Tavakolpour-Saleh, R. Razavi-Far, R. Razavi-Far, J. Zarei, M. Saif, "Genetic Algorithm-Based Sliding Mode Control of a Human Arm Model", *IFAC-PapersOnLine*, Vol. 55, No. 10, 2022, pp. 2968-2973. <https://doi.org/10.1016/j.ifacol.2022.10.183>
- [23] S. Gupta, A. Agrawal, E. Singla, "Architectural design and development of an upper-limb rehabilitation device: A modular synthesis approach", *Disability and Rehabilitation: Assistive Technology*, Vol. 19, No. 1, 2024, pp. 139-153. <https://doi.org/10.1080/17483107.2022.2071486>
- [24] R. C. de Freitas, G. R. Naik, M. J. S. Valença, B. L. D. Bezerra, R. E. de Souza, W. P. dos Santos, "Surface electromyography classification using extreme learning machines and echo state networks", *Research on Biomedical Engineering*, Vol. 38, No. 2, 2022, pp. 477-498. <https://doi.org/10.1007/s42600-022-00201-7>
- [25] Z. Ben Hazem, N. Guler, A. H. Altaif, "A study of advanced mathematical modeling and adaptive control strategies for trajectory tracking in the Mitsubishi RV-2AJ 5-DOF Robotic Arm", *Discover Robotics*, Vol. 1, No. 1, 2025, 2. <https://doi.org/10.1007/s44430-025-00001-5>
- [26] N. Mirrashid, Ü. T. E. Alibeiki, S. M. Rakhtala, "Development and control of an upper limb rehabilitation robot via ant colony optimization-PID and fuzzy-PID controllers", *International Journal of engineering*, Vol. 35, No. 8, 2022, pp. 1488-1493. <https://doi.org/10.5829/IJE.2022.35.08B.04>
- [27] H. Wang, J. Lu, "Research on fractional order fuzzy PID control of the pneumatic-hydraulic upper limb rehabilitation training system based on PSO", *International Journal of Control, Automation and Systems*, Vol. 20, No. 1, 2022, pp. 310-320. <https://doi.org/10.1007/s12555-020-0847-1>
- [28] X. Jia, B. Zhao, J. Liu, S. Zhang, "A trajectory planning method for robotic arms based on improved dynamic motion primitives", *Industrial Robot: the international journal of robotics research and application*, Vol. 51, No. 5, 2024, pp. 847-856. <https://doi.org/10.1108/IR-12-2023-0322>
- [29] Q. Li, Y. Liu, J. Zhu, Z. Chen, L. Liu, S. Yang, J. Li, R. Jin, J. Tao, L. Chen, "A motion recognition model for upper-limb rehabilitation exercises", *Journal of Ambient Intelligence and Humanized Computing*, Vol. 14, No. 12, 2023, pp. 16795-16805. <https://doi.org/10.1007/s12652-023-04688-5>
- [30] A. Eltayeb, G. Ahmed, I. H. Imran, N. M. Alyazidi, A. Abubaker, "Comparative analysis: Fractional pid vs. pid controllers for robotic arm using genetic algorithm optimization", *Automation*, Vol. 5, No. 3, 2024, pp. 230-245. <https://doi.org/10.3390/automation5030014>